Kinetic Study of the Initial Lithiation of Amorphous Silicon Thin Film Anodes

Citation: Miao, Jinghui and Carl V. Thompson, "Kinetic Study of the Initial Lithiation of Amorphous Silicon Thin Film Anodes." Journal of the Electrochemical Society 165, 3 (March 2018): A650-A656 doi. 10.1149/2.1011803jes ©2018 Authors

As Published: https://dx.doi.org/10.1149/2.1011803JES

Publisher: The Electrochemical Society

Persistent URL: https://hdl.handle.net/1721.1/128867

Version: Final published version: final published article, as it appeared in a journal, conference proceedings, or other formally published context

Kinetic Study of the Initial Lithiation of Amorphous Silicon Thin Film Anodes

Jinghui Miao and Carl V. Thompson[z]

Department of Materials Science and Engineering, Massachusetts Institute of Technology, Cambridge, Massachusetts 02139, USA

The mechanisms and kinetics of lithiation and delithiation of amorphous silicon were investigated using potentiostatic techniques and thin films of different thickness, with a focus on the initial lithiation process that occurs in the first cycle. In potentiostatic tests, distinct kinks were observed in the current vs. time curves, and the time at which the kink occurred increased for thicker films. This behavior can be explained using a model in which a sharp interface between an amorphous Li_xSi phase and Li-saturated amorphous Si propagates through the film. Using this model, the rate-limiting process was determined to be diffusion of Li in the Li_xSi phase rather than reaction at the lithiation front. The Li diffusivity in the lithiated phase was determined to be in the 10^{-13} cm^2/s range, independent of film thickness above 135 nm. The thin-film potentiostatic technique used in this study should prove useful in investigation of the mechanisms and rate parameters for other phase transitions that occur during lithiation of silicon and for kinetic studies of other electrode materials.

 [DOI: 10.1149/2.1011803jes]

Manuscript submitted December 4, 2017; revised manuscript received February 6, 2018. Published March 7, 2018.

Li-ion rechargeable batteries have been the focus of much research and development over recent decades. They power products ranging from electric vehicles to miniaturized electronic and medical devices. Due to its largest known capacity (8375 Ah/cm^3, 3579 Ah/kg), Si is viewed as a promising anode material for batteries with high energy and power densities. Its abundance and relatively low cost also make it a practically feasible anode material.[1] However, Si anodes suffer from capacity fade due to the very large volume expansion (up to 400%)[2] that occurs during lithiation and the consequent mechanical degradation it causes.[3] In storing lithium, silicon goes through a sequence of structural transitions that affect the rate at which mechanical stress develops.[4,5] This, in turn, affects the degree to which mechanical stresses can be accommodated through plastic deformation rather than fracture.[6] Hence, a detailed understanding of the nature and kinetics of structural transitions that occur during lithiation and delithiation of silicon should provide insight into means of mediating the effects of mechanical stress on the cyclability of Si anodes.

Electrochemically driven reactions between Li and Si have been studied under a variety of conditions, including at elevated and room temperature. Equilibrium titration experiments at 415°C show that four crystalline lithium silicide (Li_xSi) phases form ($Li_{12}Si_7$, Li_7Si_3, $Li_{13}Si_4$ and $Li_{22}Si_5$).[7–9] At room temperature, however, it is found using X-ray diffraction (XRD) and high resolution transmission electron microscopy (HRTEM) that the equilibrium crystalline Li-Si phases are absent and the crystalline $Li_{15}Si_4$ phase is observed only at the highest levels of lithiation.[10] At lower levels of lithiation, metastable amorphous phases are formed instead.[11] This phenomenon is similar to chemically driven solid-state amorphization reactions,[12] which are thought to be associated with higher barriers to nucleation of the crystalline phases.[13] Amorphous alloy phases with different stoichiometries have been associated with features in discharge and CV curves for Si,[14,15] and their local atomic structures have been studied using nuclear magnetic resonance (NMR), XRD and Mössbauer spectroscopy.[16–19] Distinct local atomic configurations of Li and Si have been identified at different stages of lithiation.

While crystalline Si (c-Si) and amorphous Si (a-Si) have similar electrochemical responses after the first cycle, they behave quite differently in the first cycle. Due to the large structural change from the pristine crystalline Si phase to an amorphous lithiated Si phase, the first lithiation cycle for c-Si has been widely accepted to follow a first-order phase transition mechanism, characterized by motion of a sharp interface between the crystalline and amorphous phases observed in in situ TEM[10,17,20] and X-ray reflectivity (XRR)[21] experiments. The kinetics of this process has been analyzed using an explicit three-flux kinetic model.[22,23] In contrast, the first cycle lithiation of a-Si is believed by some to be a single-phase diffusion process without a phase transition involving motion of a sharp interface.[7,20] However, in situ TEM experiments have provided evidence for a sharp interface separating unreacted a-Si and the lithiated a-Li_xSi in the initial lithiation process, in a way similar to that of c-Si in the first cycle.[23–27] This phenomenon strongly suggests that the initial lithiation of a-Si also involves a phase transition stage. In situ TEM observations are carried out using high currents and overpotentials in order to accelerate the reactions. It therefore remains possible that the mechanism of the initial lithiation of amorphous silicon is different when discharged within the normal operation window. Here we present a relatively simple electrochemical characterization methodology based on potentiostatic experiments carried out on thin films of silicon,[28–30] and apply kinetic models for analysis of the mechanisms that control the rate of lithiation in a-Si in the first and subsequent cycles.

Experimental Procedures

Double-side polished aluminum oxide (99.6%, Al_2O_3, 250 μm thick, Stellar Ceramics) was used as the substrate for a-Si thin film deposition. The aluminum oxide was cleaved into 5 mm by 8 mm pieces and was subsequently ultrasonicated for 5 min in acetone, isopropyl alcohol and deionized water to remove surface contaminants. After this step, the substrates were rinsed again in deionized water and dried using nitrogen. A 10-nm-thick titanium film was deposited on the alumina to serve as an adhesion layer and a 100-nm-thick copper film was then deposited to serve as a current collector. Amorphous Si thin films were sputtered (CMS-18 Kurt J. Lesker) onto the Cu layer under 3.1 mTorr of argon and at a 100 W RF power at room temperature. For thickness dependence studies, 135 nm, 180 nm, 225 nm, 270 nm and 315 nm thick Si samples were prepared. The thickness of the samples was measured using cross-sectional scanning electron microscopy (SEM). The as-deposited films were confirmed to be amorphous based on Raman spectroscopy.

To prepare half cells, samples were assembled into customized cells (Tomcell, Japan). Metallic Li was used as the reference electrode. The liquid electrolyte was prepared by mixing 1,3-dioxolane (DOL, Sigma-Aldrich) and bis(trifluoromethane)sulfonimide Li salt (Sigma Aldrich) to make a 1 M solution.[31] Electrodes were separated using a porous polymer separator (Celgard). Electrochemical experiments were performed using a Solartron 1470 E potentiostat.

[z]E-mail: cthomp@mit.edu

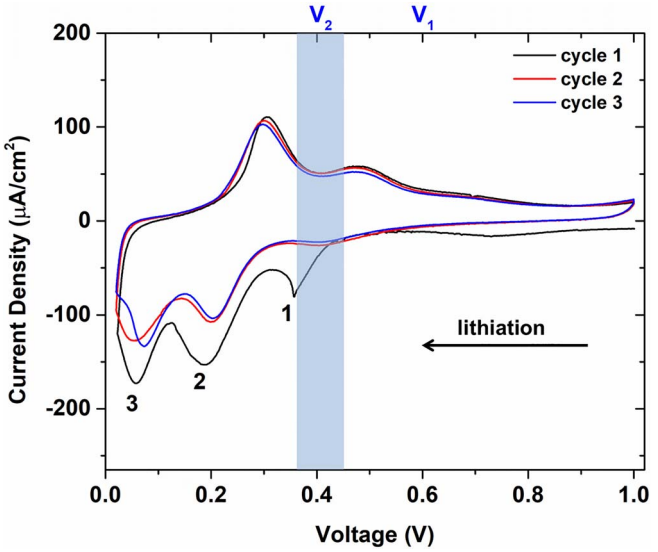

Figure 1. CV (cyclic voltammogram) curves in cycles 1–3 of a 315 nm thick a-Si thin film sample. The two voltages used in potentiostatic tests are denoted as V_1 and V_2 (in the voltage range shaded in blue). The scan rate is 40 μV/s.

Experimental Results

To investigate the lithiation characteristics of a-Si, CV tests were carried out (Figure 1). Three major peaks were observed during the initial lithiation (peak 1, 2, and 3 at 0.36 V, 0.2 V, and 0.07 V, respectively). These peaks are attributed to the formation of Li-Si alloys with varied compositions. It can be seen that peak 1 is different from the rest of the peaks in terms of its reversibility and shape. The occurrence of peak 1 at a higher potential than other reversible peaks can be explained as an initial reaction between Li and unreacted a-Si, during which the structure of the a-Si is irreversibly altered. It has also been reported in previous studies that the position of peak 1 depends on the initial structure of samples.[15,32,33] The disappearance of peak 1 in following cycles is consistent with previous results that indicate that a significant structural change occurs irreversibly in amorphous Si in the initial cycle.[25,27]

Given the CV results, potentiostatic techniques were developed to characterize the nature and rate of structural transitions associated with the CV peaks. Here we focus on peak 1 observed during the first lithiation. The system was first held at $V_1 = 600$ mV in order to isolate the irreversible lithiation process from surface reactions indicated by the shallow bump at roughly 0.75 V. After the hold at V_1, a potential jump to a second voltage V_2 was made and the current was monitored during this potentiostatic hold. Different V_2 values were selected between 360 and 440 mV (marked in blue in Figure 1) to study the rate of the structural transformation associated with peak 1 under different kinetic conditions. For purposes of comparisons, the same two-step potentiostatic test was carried out in the second cycle after full delithiation of the samples in the first cycle.

The results of potentiostatic tests under different potentials and in films with different thicknesses are shown in Figure 2. In all cases the current-time curves are marked by an abrupt kink, which divides the curves into two stages. The time at which the kink occurs is defined as t_{kink} and is determined at the local maximum of the lithiation rate ($\partial i/\partial t$). Figure 2a shows that t_{kink} depends on the applied voltage V_2. For a high applied voltage (small potential step), the kink occurs at a much later stage and the earlier stage of the reaction is extended (e.g. $V_2 = 440$ mV in Figure 2a). On the other hand, when the applied voltage is very low the kink is buried in the initial transient and becomes unobservable (data not shown). Figure 2b shows the dependence of the kink position on the initial film thickness (135, 180, 225, 270, and 315 nm) for the same potential step ($V_2 = 400$ mV), where t_{kink} decreases as the film thickness is reduced.

Discussion

Lithiation models for cycle 1 and cycle 2.—The occurrence of the kink in the current-time curve and its dependence on the initial film thickness as shown in Figure 2 are consistent with a structural transition that proceeds from the electrolyte/Si interface to the Si/current collector interface. Two models are proposed to explain the lithiation processes under potentiostatic conditions in cycle 1 and 2 (Figures 3c and 3d). We suggest that cycle 1 lithiation follows a propagating interface model as illustrated in Figure 3c and as seen in in situ TEM studies.[25,27] When the sample is initially held at V_1, Si forms a dilute solution with Li without a significant structural change (the lightest blue regime in Figure 3c, stage 1-1). After the potential jump to V_2 , reduction of additional Li ions leads to an accumulation and subsequent insertion of Li atoms at the Si surface and a new a-Li_xSi phase nucleates and grows into a continuous layer (the darker blue regime in Figure 3c, stage 1–2). Formation of the new phase involves Si-Si bond breaking in the initially dense Si network, in a similar way to chemically-drive solid state amorphization reactions.[27,34] The volume

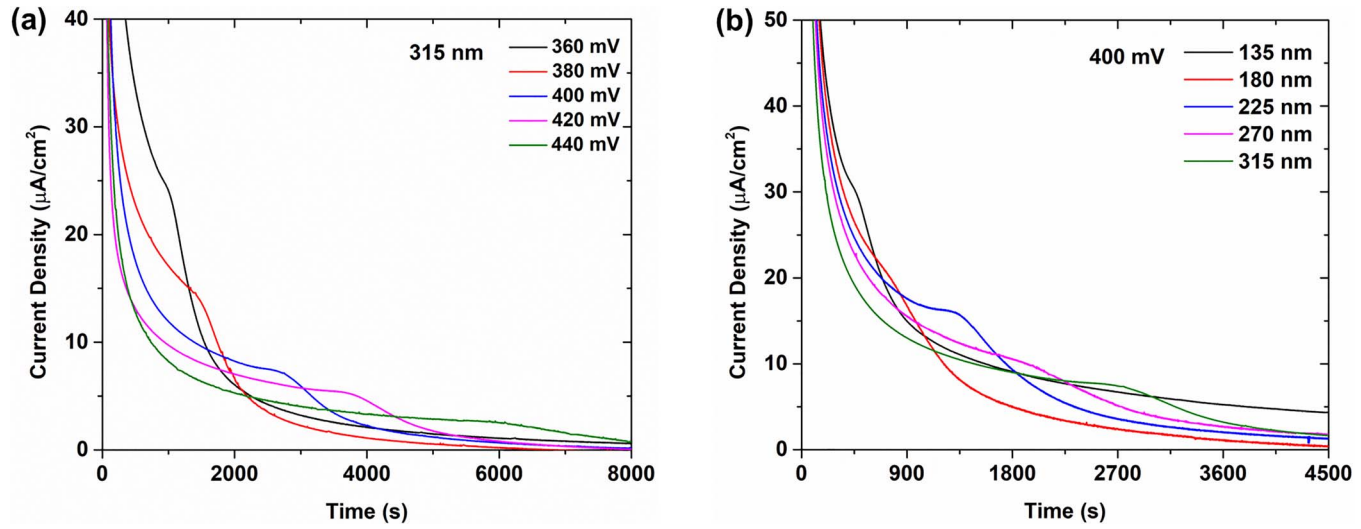

Figure 2. Current-time curves for (a) different values of V_2 in 315 nm thick films, and (b) at $V_2 = 400$ mV in a-Si films of different thicknesses. For convenience the signs of the current densities in all potentiostatic tests are taken as positive. All data were collected in cycle 1.

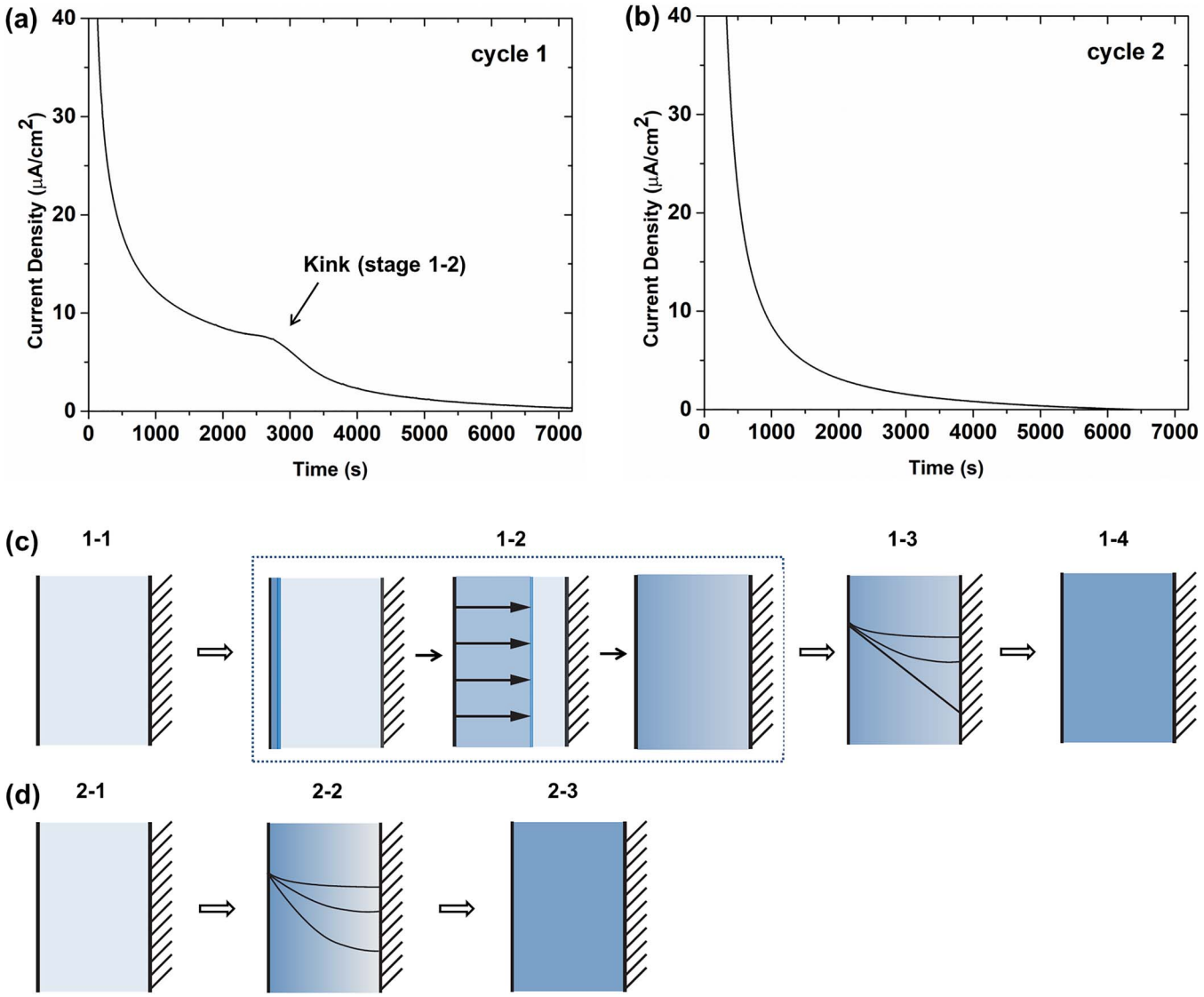

Figure 3. (a) and (b) Current-time curves for 315 nm thick films for $V_2 = 400$ mV in cycle 1 and 2, respectively. (c) and (d) schematics illustrating the propagating interface model (cycle 1), and the single-phase diffusion model (cycle 2), respectively. Contrasts in the shading reflect Li concentration differences. Evolution of Li concentration profiles based on the models are shown as lines in 1–3 and 2–2.

of new phase then increases by propagation of a planar a-LixSi/a-Si interface across the thickness of the film from the surface facing the electrolyte to the interface with the current collector. Once the a-Li_xSi/a-Si interface reaches the current collector, the rate of lithiation suddenly drops which results in the kink in potentiostatic curves. Stage 1–2 is therefore seen as a phase transition from the a-Si solid solution to the a-Li_xSi phase, rather than a simple diffusion process. At the end of stage 1–2 the film is composed of the single-phase a-Li_xSi. We propose that at this point, a Li concentration gradient exists in the a- Li_xSi, and that the current observed after the kink is associated with continued Li insertion to reach a uniform composition across the thickness of the a- Li_xSi (Figures 3c 1–3, 1–4). In contrast, cycle 2 follows a simpler lithiation model (Figure 3d). After cycle 1 the expansion and structural change in the a-Si network is partially retained[17,25,35] and at the same applied voltage V_2, Li atoms can more easily diffuse through and occupy interstitial sites without causing a phase transition (Figures 3d 2-2, 2–3). This single-phase diffusion model is consistent with the absence of the kink in the current-time curves in cycle 2.

It should be noted that SEI (solid electrolyte interphase) formation does not appear to play a significant role in the results described above, as supported by the following observations. First, as shown in Figure S1 in the supplemental information, the initial current in cycle 2 is much larger than the current in cycle 1, and there is no significant difference in the capacity changes in the two cycles corresponding to the potential step in Figure S1. These results suggest that SEI formation in cycle 1 is either effectively suppressed by the hold step at 600 mV, or only plays a minor role in the selected potential regime (360–440 mV). Second, the initial lithiation does not lead to penetrating cracks where SEI can be further formed.[3] Therefore, the thickness dependence of t_{kink} in Figure 2b cannot be related to SEI formation, but instead must be related to a bulk transition. Third, Figure S2 in the supplemental information shows that potentiostatic tests of samples coated with lithium phosphorus oxynitride (LiPON) as an artificial SEI layer to suppress SEI formation,[4,36,37] yield similar results. This again supports the proposed model in which the kink is correlated with lithiation of Si.

Quantitative analysis and model testing.—Quantitative analyses are needed to test the qualitative models described above. Here we develop a propagating interface model for the initial lithiation of a planar a-Si film with the quantities defined in Figure 4. This model

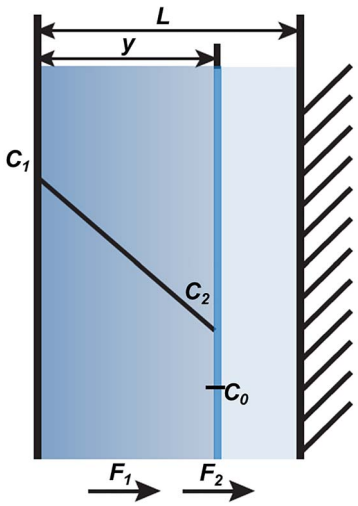

Figure 4. Schematic for quantitative analysis of the propagating interface model (stage 1–2 in Figure 3). The dark blue region is the a-Li$_x$Si phase and light blue region is the a-Si(Li) solution. (See below for term clarifications.).

is analogous to models developed for chemically driven reactive film formation[34,38] and is similar to extensions of this approach to electrochemical film formation.[22,23] The initial lithiation within the selected voltage range is assumed to involve four processes: (1) Li ions are transported through the liquid electrolyte to the electrolyte-Si interface, (2) the Li ions are reduced and react to alloy with Si at the electrolyte-Si interface, (3) once a continuous layer of silicide is formed Li diffuses across the silicide layer, and (4) Li reacts with unreacted Si to form more silicide. We will assume that Li transport through the electrolyte and charge transfer at the electrolyte interface are not rate limiting and consider only the diffusive flux of Li through Li$_x$Si to the Li$_x$Si/a-Si interface, F_1 in Figure 4, and the reaction flux at the Li$_x$Si/Si interface, F_2, as potentially rate limiting. C_1 is the concentration of Li in Li$_x$Si at the electrolyte/Li$_x$Si interface, which is in equilibrium with the applied voltage V_2. C_2 is the actual Li concentration at the Li$_x$Si/Si interface, and C_0 is the concentration of Li in Li$_x$Si if it was in equilibrium with the a-Si solid solution. L is the initial thickness of the Si film and y is the thickness of the Li$_x$Si layer at any given time.

Under steady state conditions the concentration profile across Li$_x$Si can be taken to be linear, as illustrated in Figure 4, so that Fick's law gives

$$F_1 = D_{Li}\frac{C_1 - C_2}{y}, \quad [1]$$

where D_{Li} is the diffusivity of Li in Li$_x$Si. As mentioned above, under potentiostatic conditions and given fast reactions in the electrolyte and at the surface, C_1 can be taken as a constant equal to the equilibrium Li concentration in Li$_x$Si corresponding to the applied voltage[39] while C_2 changes with time.[38]

At the Li$_x$Si/Si interface, Li reacts with Si to form Li$_x$Si and the lithiation front moves toward the contact layer. This first-order chemical reaction is driven by the excess Li at the interface and can be described by

$$F_2 = k(C_2 - C_0), \quad [2]$$

where k is a reaction rate constant, and $(C_2 - C_0)$ describes the excess Li concentration in the Li$_x$Si at the Li$_x$Si/Si interface. It is hard to obtain an accurate value of C_0, but it can be approximated by the average concentration of Li in Si dilute solution before the potential step to V_2.

Under steady state conditions, the two fluxes should be equal. From Eqs. 1 and 2, C_2 is found to be

$$C_2 = \frac{D_{Li}C_1 + kC_0}{ky + D_{Li}} \quad [3]$$

and the flux is given by

$$F = F_1 = F_2 = \frac{\left(\frac{D_{Li}}{y}\right)k(C_1 - C_0)}{\frac{D_{Li}}{y} + k}. \quad [4]$$

The total flux is proportional to the thickening rate of the Li$_x$Si as given by

$$i\,(t) = \mathcal{F}F = \mathcal{F}(C_1 - C_0)\frac{\left(\frac{D_{Li}}{y}\right)k}{\frac{D_{Li}}{y} + k}, \quad [5]$$

where $\mathcal{F}$ is Faraday's constant, and $(C_1 - C_0)$ here is the approximate average concentration of the newly formed Li$_x$Si phase, which is used to convert mass flux into current.

In most experimental regimes, the overall transformation rate is dominated by a rate-limiting step. Based on Eq. 5, there are two possible scenarios:

(1) Reaction-limited thickening ($k \ll D_{Li}/y$), which gives

$$i\,(t) \approx \mathcal{F}(C_1 - C_0)k. \quad [6]$$

(2) Diffusion-limited thickening ($k \gg D_{Li}/y$), which gives:

$$i\,(t) \approx \mathcal{F}(C_1 - C_0)\frac{D_{Li}}{y}. \quad [7]$$

With all kinetic parameters (k, D_{Li}) and concentration terms (C_1, C_0) being constant, the two scenarios generate very different current-time relations. If the process is reaction limited, the current should be independent of time, whereas if it is diffusion limited the current should decrease with increasing Li$_x$Si thickness and time. Given the behavior shown in Figure 3a, the phase transition process before the kink must be limited by Li diffusion in the new Li$_x$Si phase. By solving Eq. 7 we can obtain expressions for the thickness of Li$_x$Si and the current as functions of time

$$y\,(t) = \sqrt{2D_{Li}t + y_0^2} \quad [8]$$

and

$$i\,(t) = \mathcal{F}(C_1 - C_0)\sqrt{\frac{D_{Li}}{2}}\left(t + \frac{y_0^2}{2D_{Li}}\right)^{-1/2}, \quad [9]$$

where y_0 is the initial thickness of Li$_x$Si after formation of a layer through coalescence of nuclei. For thick films we can assume $y_0 \ll L$, so that Eqs. 8 and 9 can be rearranged to give

$$y\,(t) = \sqrt{2D_{Li}t} \quad [10]$$

and

$$i\,(t) = \mathcal{F}(C_1 - C_0)\sqrt{\frac{D_{Li}}{2}}t^{-1/2}. \quad [11]$$

The single-phase diffusion model, which accounts for stage 2-2 in Figure 3c, can be treated as a diffusion process under a potentiostatic condition at the Si/electrolyte interface, and an impermeable-boundary (zero-flux) condition at the Si/current collector interface. The current-time relations in short-time ($t \ll l^2/D_{Li}$) and long-time ($t \gg l^2/D_{Li}$) limits are given by[39,40]

$$i\,(t) = \frac{Q}{L}\left(\frac{D_{Li}}{\pi}\right)^{1/2}t^{-1/2} \quad [12]$$

and

$$i\,(t) = \frac{2QD_{Li}}{L^2}\exp\left(-\frac{\pi^2 D_{Li}}{4l^2}t\right), \quad [13]$$

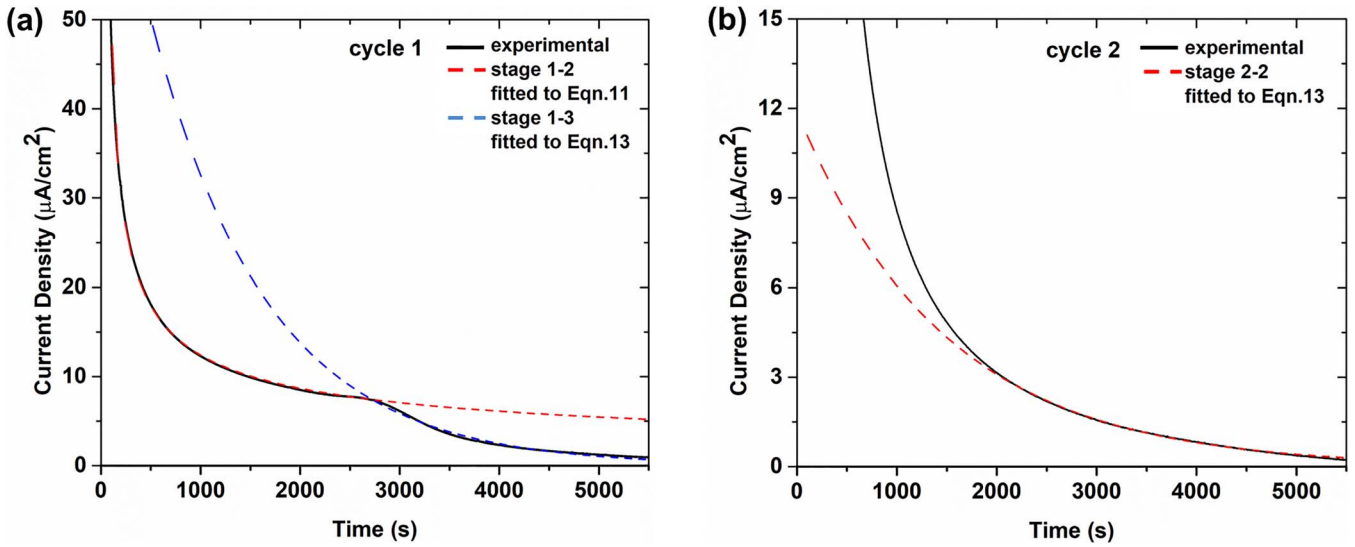

Figure 5. Experimental and fitted data for potentiostatic tests at $V_2 = 400$ mV in (a) cycle 1 and (b) cycle 2 for the 315 nm thick samples (solid lines indicate experimental data and dashed lines indicate fitting results).

respectively, where Q is the total amount of charge transferred during lithiation. For fitting purposes Eq. 13 is used to avoid the complexity of transient processes in the short-time regime. It is worth noting that fitting data from stage 1–3 to Eq. 13 is an approximate treatment because at the end of the propagation stage the concentration profile is not the same as that predicted by the single phase diffusion model.

Figure 5 shows fits to the equations discussed above along with experimental data for cycles 1 and 2 potentiostatic tests at $V_2 = 400$ mV. For cycle 1 (Figure 5a), Eq. 11 is fit to the data for $t < t_{kink}$ and Eq. 13 is fit to the data for $t > t_{kink}$. For cycle 2 (Figure 5b), Eq. 13 is fit in the long–time regime from $t = 2000$ s on. The R-square value for all fitting results are larger than 0.99, indicating consistency between models and experiments.

In Figure 2c, there is a clear correlation between t_{kink} and the initial thickness of the films, which is presented more clearly in Figure 6. Under three potential steps the slopes of $\ln(t_{kink})$ vs. ln(thickness) curves are approximately two. This again supports the diffusion-limited interface propagation model in cycle 1 instead of a reaction-limited model, for which the slope would be one.

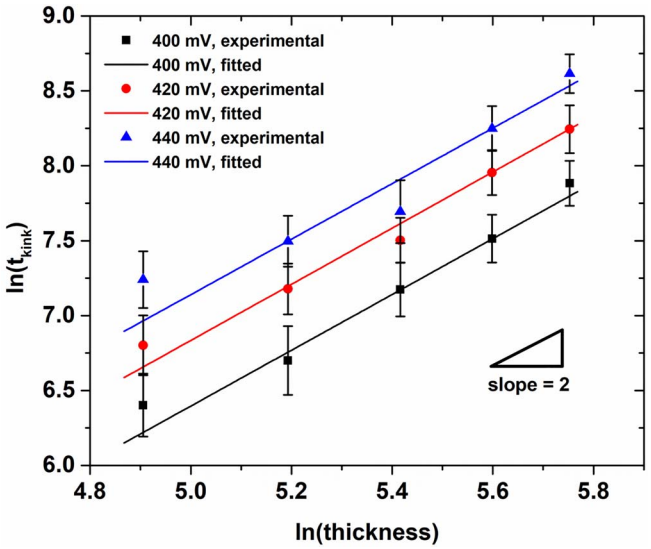

Figure 6. Experimental and fitted data for $\ln(t_{kink})$ vs. ln(film thickness) for potentiostatic experiments carried out at $V_2 = 400$, 420, and 440 mV.

The proposed propagating interface model for the initial lithiation is supported by experimental data, and also in agreement with reported in situ TEM studies.[23,25,27] The existence of an interface between unlithiated a-Si and lithiated a-Li_xSi, observed using in situ TEM and the film thickness dependence of the kink feature observed in potentiostatic tests, validates that phase separation with a sharp interface governs the initial lithiation process, rather than single-phase diffusion. However, a noteworthy difference between the interpretation given for in-situ TEM experiments and our experiments is the rate limiting step for the initial lithiation. Our potentiostatic experiments show a $t^{-1/2}$ dependence of the current (for $t < t_{kink}$), which strongly suggests a diffusion limited process, whereas in situ TEM studies have been interpreted to indicate an interface-reaction limited process. Possible explanations for such difference include that: (1) the applied voltage in in situ TEM studies is much lower[23–27] than the voltage in our case and this possibly leads to formation of a more Li-rich Li_xSi final phase with faster transport kinetics; (2) our samples are room temperatures sputtered, while the in situ TEM samples were fabricated at elevated temperature using CVD techniques, which could affect the activation barrier for diffusion of Li in Li_xSi;[6,41,42] (3) the mechanical stress that develops in our thin film geometry is sufficiently different form the stress state that develops in the nanoparticles and nanowires used in in situ TEM studies to affect the relevant kinetic parameters, especially in regimes in which accumulated stress causes the transformation to end before completion.[23]

The diffusivity of Li in Li_xSi.—By fitting data to Eq. 9 as discussed above, values for the diffusivity of Li in Li_xSi in cycle 1 can be determined as a function of V_2 for different film thicknesses, leading to the results shown in Figure 7. These diffusivities are on the order of 10^{-13} cm^2/s, which is within one order of magnitude of reported values based on EIS, GITT and PITT techniques.[43–45] The diffusivity vs. thickness curves have similar trends for all three values of V_2 (400, 420, and 440 mV). For thicknesses above 135 nm, diffusivities remain relatively constant with only a slight decrease with film thickness. However, for the thinnest 135 nm thick films, the diffusivities are larger than those determined for the thicker films. This may be an indication that the assumptions of the model are no longer satisfied at thicknesses of 135 nm and below, e.g. that $y_0 \ll L$, and that a steady state regime is attained. However, it should be noted that in the 135 nm films, the kink is observed at much shorter times than for thicker films. This makes fitting of the pre-kink stage less precise as

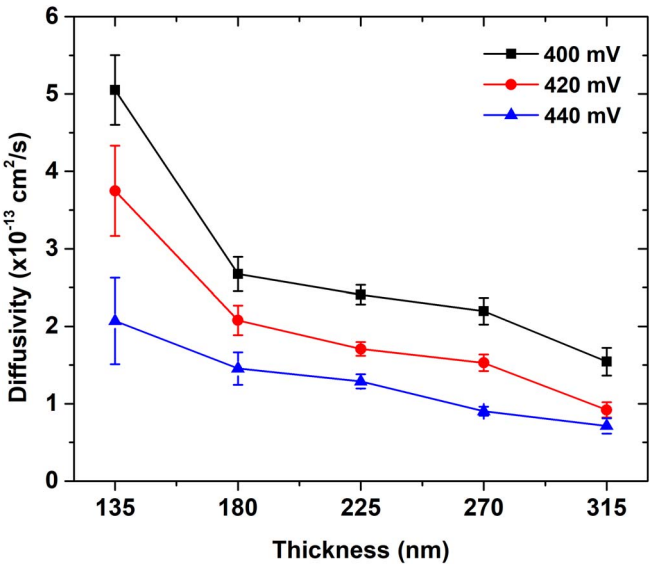

Figure 7. Li diffusivity in Li_xSi vs. film thickness curves, for diffusivities determined using the propagating interface model in cycle 1.

the kink is more difficult to distinguish in the current-time data. The variations in the diffusivities determined for the 135 nm films may therefore be associated with larger measurement errors.

The diffusivity values in Figure 8 are within the same order of magnitude, suggesting that the diffusion processes in cycle 1 and 2 are similar, which is consistent with assumption that Li atoms diffuse through the Li_xSi phase during the phase transition and during the second cycle. A small voltage dependence of the calculated diffusivities is observed only for cycle 1, when the phase transition occurs. To understand this voltage dependence, we need to recall the Nernst equation, which shows a straightforward relationship between the applied voltage and the equilibrium concentration of Li in Li_xSi:

$$V_2 = -\frac{RT}{\mathcal{F}} ln\gamma_{Li} C_{Li,\ eq}\ , \qquad [14]$$

where R is the gas constant, γ_{Li} is the activity coefficient of Li in the formed phase, and $C_{Li,\ eq}$ is the equilibrium concentration of Li

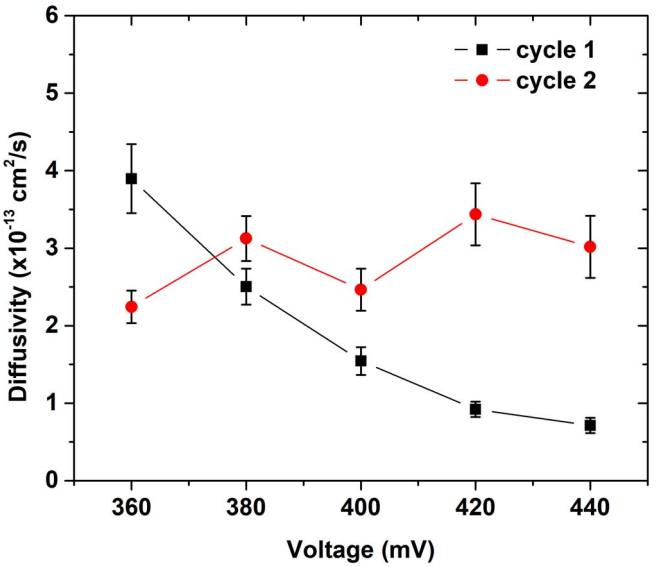

Figure 8. Diffusivity vs. voltage curves determined using (a) the propagating interface model in cycle 1 and (b) the single phase diffusion model in cycle 2.

in the Li_xSi phase at the applied voltage V_2. Eq. 14 indicates that a lower voltage leads to a higher Li concentration. Since the Si-Si bonds are more rigid than Li-Li bonds, during lithiation when Li atoms have more Li atoms instead of Si atoms as nearest neighbors, the ionicity of Li-Si bonds increases[46] and the matrix becomes softer. The diffusion of Li atoms requires jumping via interstitial sites in the amorphous matrix, and the increase in diffusivity with decreased voltage can thus be interpreted as a smaller diffusion barrier as a result of a more pliable matrix and larger repulsive force exerted on the diffusing atoms by the surrounding Li neighbors.[41,47] For cycle 2, however, the diffusivity values do not show an obvious dependence of voltage. We believe this is due to the more open matrix and a less compressive stress developed within the tested voltage range in cycle 2 after the large irreversible structural change in cycle 1.[4,10]

Conclusions

In summary, we present a simple potentiostatic technique for kinetic studies of the initial lithiation of amorphous Si thin films. During potentiostatic testing of films, a kink feature is observed during the first lithiation process. The time at which this kink appears increases when thicker films are used. This suggests that the initial lithiation processes occurs through propagation of a reaction front from the film-electrolyte surface to the film-substrate surface. We propose that an amorphous Li_xSi phase is formed at the electrolyte/Si surface and that this phase grows through propagation of a sharp interface between it and the a-Si. A two-step potentiostatic experimental procedure was used to test this model. Pristine films were first held at a relatively high voltage $V_1 = 600$ mV, and different samples were abruptly stepped down to different voltages (V_2), ranging from 360–440 mV, for potentiostatic measurements of the current versus time. By fitting experimental data with a propagating interface model, we find that the rate limiting step in this voltage range is diffusion of Li in the newly formed phase, not the reaction at the Li_xSi/Si interface. The propagating interface model can also be used to determine the diffusivity of Li in the Li_xSi phase as a function of the initial film thickness and of the voltage V_2 and of the film thickness. The diffusivity values determined in this way have only a weak dependence on the initial film thickness. The diffusivity was found to have a weak dependence on the applied voltage, which may be the result of local structural changes during the initial lithiation process. In the second lithiation cycle, the kink is absent and lithiation appears to occur via a single-phase diffusion process. Through these studies it can be seen that our two-step thin film testing technique allows determination of the nature of lithiation processes and extraction of kinetic factors such as diffusivity.

Acknowledgments

This work was supported by the National Research Foundation, Prime Minister's Office, Singapore under its Campus for Research Excellence and Technological Enterprise (CREATE) program, through the Singapore-MIT Alliance for Research and Technology (SMART), Low Energy Electronic Systems (LEES) Interdisciplinary Research Group (IRG) and by the Skoltech Center for Electrochemical Energy Storage.

References

1. C.-X. Zu and H. Li, *Energy & Environmental Science*, **4**(8), 2614 (2011).
2. B. Jerliu, E. Hüger, L. Dorrer, B.-K. Seidlhofer, R. Steitz, V. Oberst, U. Geckle, M. Bruns, and H. Schmidt, *The Journal of Physical Chemistry C*, **118**(18), 9395 (2014).
3. L. Beaulieu, K. Eberman, R. Turner, L. Krause, and J. Dahn, *Electrochemical and Solid-State Letters*, **4**(9), A137 (2001).
4. A. Al-Obeidi, D. Kramer, S. T. Boles, R. Mönig, and C. V. Thompson, *Applied Physics Letters*, **109**(7), 071902 (2016).
5. M. J. Chon, V. A. Sethuraman, A. McCormick, V. Srinivasan, and P. R. Guduru, *Physical Review Letters*, **107**(4), 045503 (2011).
6. K. Zhao, G. A. Tritsaris, M. Pharr, W. L. Wang, O. Okeke, Z. Suo, J. J. Vlassak, and E. Kaxiras, *Nano letters*, **12**(8), 4397 (2012).
7. R. A. Huggins, *Journal of Power Sources*, **81**, 13 (1999).

8. H. Okamoto, *Journal of Phase Equilibria*, **11**(3), 306 (1990).
9. C. J. Wen and R. A. Huggins, *Journal of solid state chemistry*, **37**(3), 271 (1981).
10. M. Obrovac and L. Christensen, *Electrochemical and Solid-State Letters*, **7**(5), A93 (2004).
11. P. Limthongkul, Y.-I. Jang, N. J. Dudney, and Y.-M. Chiang, *Acta Materialia*, **51**(4), 1103 (2003).
12. R. Schwarz and W. Johnson, *Physical Review Letters*, **51**(5), 415 (1983).
13. C. V. Thompson, *Journal of materials research*, **7**(2), 367 (1992).
14. J. Li and J. Dahn, *Journal of The Electrochemical Society*, **154**(3), A156 (2007).
15. M. Obrovac and L. Krause, *Journal of The Electrochemical Society*, **154**(2), A103 (2007).
16. B. Key, R. Bhattacharyya, M. Morcrette, V. Seznec, J.-M. Tarascon, and C. P. Grey, *Journal of the American Chemical Society*, **131**(26), 9239 (2009).
17. B. Key, M. Morcrette, J.-M. Tarascon, and C. P. Grey, *Journal of the American Chemical Society*, **133**(3), 503 (2010).
18. J. Li, A. Smith, R. Sanderson, T. Hatchard, R. Dunlap, and J. Dahn, *Journal of The Electrochemical Society*, **156**(4), A283 (2009).
19. K. Ogata, E. Salager, C. Kerr, A. Fraser, C. Ducati, A. Morris, S. Hofmann, and C. P. Grey, *Nature communications*, **5**, (2014).
20. M. T. McDowell, S. W. Lee, W. D. Nix, and Y. Cui, *Advanced Materials*, **25**(36), 4966 (2013).
21. C. Cao, H.-G. Steinrück, B. Shyam, K. H. Stone, and M. F. Toney, *Nano letters*, **16**(12), 7394 (2016).
22. M. Pharr, K. Zhao, X. Wang, Z. Suo, and J. J. Vlassak, *Nano letters*, **12**(9), 5039 (2012).
23. X. H. Liu, F. Fan, H. Yang, S. Zhang, J. Y. Huang, and T. Zhu, *Acs Nano*, **7**(2), 1495 (2013).
24. X. H. Liu, J. W. Wang, S. Huang, F. Fan, X. Huang, Y. Liu, S. Krylyuk, J. Yoo, S. A. Dayeh, and A. V. Davydov, *Nature nanotechnology*, **7**(11), 749 (2012).
25. M. T. McDowell, S. W. Lee, J. T. Harris, B. A. Korgel, C. Wang, W. D. Nix, and Y. Cui, *Nano letters*, **13**(2), 758 (2013).
26. M. T. McDowell, S. W. Lee, C. Wang, W. D. Nix, and Y. Cui, *Advanced Materials*, **24**(45), 6034 (2012).
27. J. W. Wang, Y. He, F. Fan, X. H. Liu, S. Xia, Y. Liu, C. T. Harris, H. Li, J. Y. Huang, and S. X. Mao, *Nano Letters*, **13**(2), 709 (2013).
28. J. L. Allen, T. R. Jow, and J. Wolfenstine, *Chemistry of materials*, **19**(8), 2108 (2007).
29. M. Tang, W. C. Carter, and Y.-M. Chiang, *Annual Review of Materials Research*, **40**, 501 (2010).
30. Z. Wang, H. Kan, Z. Shi, B. Gao, Y. Ban, and X. Hu, *Journal of materials science & technology*, **24**(6), 915 (2008).
31. V. Etacheri, U. Geiger, Y. Gofer, G. A. Roberts, I. C. Stefan, R. Fasching, and D. Aurbach, *Langmuir*, **28**(14), 6175 (2012).
32. S. Komaba, F. Mikami, T. Itabashi, M. Baba, T. Ueno, and N. Kumagai, *Bulletin of the Chemical Society of Japan*, **79**(1), 154 (2006).
33. J. Maranchi, A. Hepp, and P. Kumta, *Electrochemical and solid-state letters*, **6**(9), A198 (2003).
34. K. Tu, *Applied Physics Letters*, **27**(4), 221 (1975).
35. C. Cao, H. G. Steinrück, B. Shyam, and M. F. Toney, *Advanced Materials Interfaces*, **4**(22), (2017).
36. A. Al-Obeidi, D. Kramer, C. V. Thompson, and R. Mönig, *Journal of Power Sources*, **297**, 472 (2015).
37. J. Li, N. J. Dudney, J. Nanda, and C. Liang, *ACS applied materials & interfaces*, **6**(13), 10083 (2014).
38. B. E. Deal and A. Grove, *Journal of Applied Physics*, **36**(12), 3770 (1965).
39. S.-I. Pyun, H.-C. Shin, J.-W. Lee, and J.-Y. Go, *Electrochemistry of insertion materials for hydrogen and lithium*, Springer Science & Business Media (2012).
40. J. Li, X. Xiao, F. Yang, M. W. Verbrugge, and Y.-T. Cheng, *the Journal of Physical Chemistry C*, **116**(1), 1472 (2011).
41. J. Moon, B. Lee, M. Cho, and K. Cho, *Journal of Power Sources*, **272**, 1010 (2014).
42. P. Johari, Y. Qi, and V. B. Shenoy, *Nano letters*, **11**(12), 5494 (2011).
43. N. Ding, J. Xu, Y. Yao, G. Wegner, X. Fang, C. Chen, and I. Lieberwirth, *Solid State Ionics*, **180**(2), 222 (2009).
44. J. Xie, N. Imanishi, T. Zhang, A. Hirano, Y. Takeda, and O. Yamamoto, *Materials Chemistry and Physics*, **120**(2), 421 (2010).
45. T. Kulova, A. Skundin, Y. V. Pleskov, E. Terukov, and O. Kon'Kov, *Journal of Electroanalytical Chemistry*, **600**(1), 217 (2007).
46. V. Shenoy, P. Johari, and Y. Qi, *Journal of Power Sources*, **195**(19), 6825 (2010).
47. J. Pan, Q. Zhang, J. Li, M. J. Beck, X. Xiao, and Y.-T. Cheng, *Nano Energy*, **13**, 192 (2015).